Modelling of ultrasound transmission through a solid-liquid interface comprising a network of gas pockets

K. Paumel, J. Moysan, D. Chatain, G. Corneloup, F. Baqué

Modelling of ultrasound transmission through a solid-liquid interface comprizing a network of gas pockets.

K. Paumel[1], J. Moysan[2], D. Chatain[3], G. Corneloup[2], F. Baqué[1]

1. CEA, DEN, Nuclear Technology Department, F-13108 Saint-Paul-lez-Durance, France.

2. Laboratoire de Caractérisation Non Destructive, Université de la Méditerranée, IUT Aix-en-Provence, Avenue Gaston Berger, 13625 Aix-en-Provence, France

3. CNRS, Aix-Marseille Université, CINAM-UPR3118, Campus de Luminy, Case 913, 13288 Marseille cedex 09

Email corresponding author : joseph.moysan@univmed.fr

Abstract

Ultrasonic inspection of sodium-cooled fast reactor requires a good acoustic coupling between the transducer and the liquid sodium. Ultrasonic transmission through a solid surface in contact with liquid sodium can be complex due to the presence of microscopic gas pockets entrapped by the surface roughness. Experiments are run using substrates with controlled roughness consisting of a network of holes and a modelling approach is then developed. In this model a gas pocket stiffness at a partially solid-liquid interface is defined. This stiffness is then used to calculate the transmission coefficient of ultrasound at the entire interface. The gas pocket stiffness has a static, as well as an inertial component, which depends on the ultrasonic frequency and the radiative mass.

PACS : 43.35.Zc, 81.70.Cv, 68.08.Bc, 28.41.Rc, 81.70.-q, 68.08.-p

Key words: ultrasounds, wetting, interface, spring model, sodium fast reactor, non destructive testing

1. Introduction

Fast neutron reactors cooled with liquid sodium (SFR reactors) are envisaged in France in the realm of fourth generation nuclear systems. Amongst the research and development topics related to this technology[1], the improvement of in-service inspection capabilities was identified as a major issue[2]. In this field, ultrasonic techniques are planned for continuous monitoring and periodical examinations of reactor components[3]. For example it will be necessary to use ultrasonic telemetry to check if components have not undergone unacceptable displacements or deformations. One of the techniques consists in using ultrasonic transducers directly immersed in liquid sodium. Research studies are currently being conducted to understand the phenomena governing the acoustic coupling of the transducer with liquid sodium, i.e. the ultrasonic transmission at the interface between the active face of the transducer and the liquid sodium in contact [4,5].

Ultrasonic transmission through solid surfaces in contact with liquid sodium is sometimes difficult, when the wetting of the sodium on the solid surface is poor (contact angle larger than 90°). It is thought that the presence of microscopic gas pockets, trapped in the irregularities (or cavities) of the surface roughness of the solid (the active face of the transducer) in contact with the liquid sodium, could be responsible for this poor acoustic coupling [6,7]. The aim of our study is to predict the ability of ultrasound waves to traverse a composite interface, i.e. a solid-liquid interface including gas pockets.

This study has some points in common with numerous other studies modelling the transmission / reflection of ultrasound at a partial contact interface. Distributed spring models are useful tools for predicting the reflection or transmission coefficient through such partial contact interface. In this field, Kendall and Tabor[8] introduce the notion of interface stiffness. The concept of a distributed spring at the interface, describing the contact behaviour, was introduced by Tattersall[9] , Baik and Thompson[10] developed a quasi-static model which is an extension of that of Tattersall, since it includes the influence of the interface's mass. Baltazar et al.[11] extended the spring model, by using normal and transverse springs to predict the reflection coefficient at a rough interface between two solids, for normal, but also oblique angles of incidence.

The description of partial contact interfaces, based on the spring model, or more generally on the mass-spring model, are applicable to various domains including the characterisation of a network of cracks, pores or coplanar inclusions[10,12], rough contact between two solids[13-17]; the strength of adhesive bonds[9,18,19];

the possible non detection of cracks under compressive load[20]; or the determination of the thickness of oil films in roller bearings[21]. Such models are now developed to take also into account non linear behaviour[22,23].

There are also numerous studies on the behaviour of gas pockets under quasi-static or dynamic pressure where the physical modelling is also based on a spring model. Liquid-vapour surface tension and pressure are two of the main parameters[24,25]. Other works in sonochemistry analyse the role of ultrasonic pressure on the contact angle[26].

Our work is at the edge between these two sets of studies. The originality of our study consists in defining a mass-spring model approach where an equivalent stiffness is calculated to model the behaviour of gas pockets distributed along a plane interface.

To the best of our knowledge, there is no example in the literature, of an application of this model to the characterisation of a partial contact interface such as a composite interface, between a solid and a liquid. The present study thus involves establishing a law to describe the behaviour of a composite interface.
In part 2 we have undertaken a simulated study, using water as the liquid, and hydrophobic silica-silicon substrates for the solid surfaces, characterized by a network of small calibrated holes, which remain filled with gas when the surface is brought into contact with water. In a previous study[5], it has been demonstrated that the gas area fraction of the composite interface does not vary under the influence of ultrasound in the present experimental conditions.

The experimental work is complemented by a theoretical approach intended to start a predictive approach. In the model the interface is considered to be a partial contact interface between the liquid and the solid. This assumption allows developing a distributed mass and spring model to determine the transmission coefficient of the interface. The major idea is to propose a description of the behaviour of a gas pocket under the influence of ultrasound to determine the stiffness of the distributed equivalent spring of the entire interface.

2. Experiment

2.1 Objectives and principle

The experiment developed is based on an immersion measurement technique. In the present study, the measurement principle consists in comparing the transmission through a composite interface (a "rough" hydrophobic sample) with that through a complete solid-liquid interface (reference sample). The aim of this approach is to eliminate any cause of transmitted signal variation arising from the measurement chain, which could be induced by any other source than the studied interface. This comparison can be characterized by the transmission mode Interface Transfer Function, FTI_t, defined as follows:

$$FTI\_t(f) = \frac{\left|\left(A^T\right)_{rh}(f)\right|}{\left|\left(A^T\right)_{ref}(f)\right|} = \frac{\left|t^{rh}(f)\right|}{\left|t^{ref}(f)\right|} \quad (1)$$

Where $|A^T(f)|$ is the modulus of the Fourier transform of the ultrasonic signal, transmitted through the considered sample at the frequency f, and $|t(f)|$ is the modulus of the transmission coefficient of the considered interface at the frequency f. The ‘rh’ subscript and exponent terms refer respectively to the studied sample and the "rough" hydrophobic interfaces, and the ‘ref’ subscript and exponent terms refer respectively to the reference sample and to the smooth interface. As the temporal signal is not monochromatic, it is more useful to make use of ultrasonic spectroscopy, i.e. to perform the analyses via the Fourier transform of the signal.

Thus, for an interface whose FTI_t value is close to 1, the acoustic coupling can be considered to be very good, whereas if FTI_t is close to zero, it will be considered to be very poor. This parameter is also used in our model, in order to compare the numerical results with those derived from the experiment.

The method used to measure the transmission coefficients for the samples involves coupling the measurements carried out with the reference sample with measurements carried out with the "rough" samples, using the same method. This method involves generating and measuring echoes, which are transmitted through the sample, first in one direction, then in the other. This allows the influence of the direction of ultrasound propagation to be studied, with respect to the "rough" side of the samples, without the need to reverse the sample positioning between two measurements (Fig. 1).

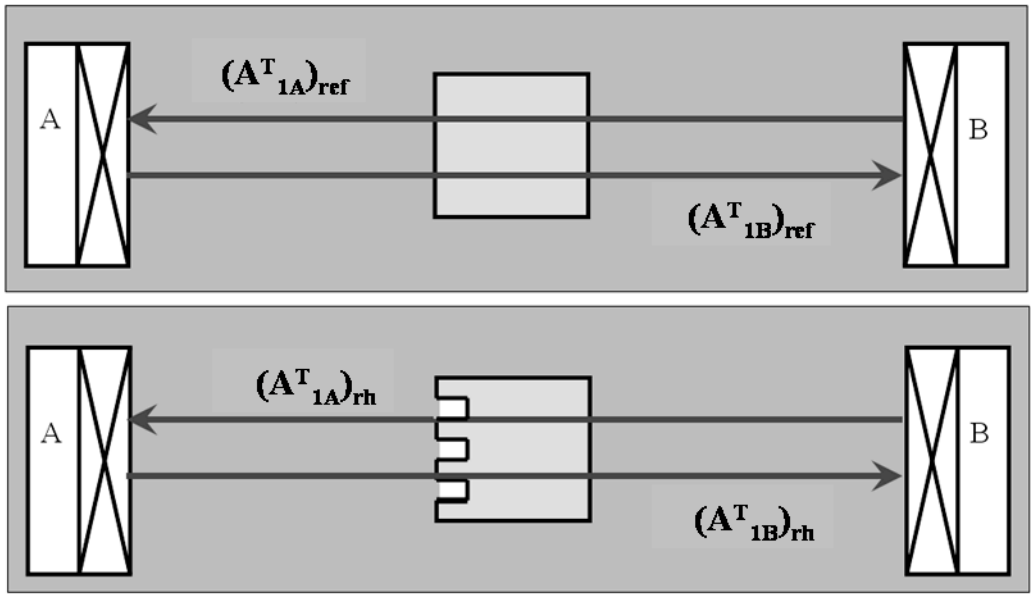

Figure 1. Path of ultrasound signals through the reference sample (ref) and through a hydrophobic "rough" sample (rh).

For the reference sample, and for each "rough" sample, two signals are transmitted through the sample, and thus need to be measured. The first corresponds to the signal for which transducer A is the emitter, i.e. the signal comprising the echo A^T_{1B} (ref or rh), and the second corresponds to the signal for which transducer B is the emitter, i.e. the signal comprising the echo A^T_{1A} (ref or rh). By expressing the problem in the form of equations, the transmission coefficients can be derived in the liquid-to-solid direction (trajectory from A to B), and in the solid-to-liquid direction (trajectory from B to A). The 'S' subscripts refer to the solid, i.e. to silicon, the 'L' subscripts refer to the liquid, i.e. water, and the 'G' subscripts refer to the gas, i.e. air.

$$t^{rh}_{pLS}(f) = \frac{\left|\left(A^T_{1B}\right)_{rh}(f)\right|}{\left|\left(A^T_{1B}\right)_{ref}(f)\right|}\left|t^{ref}_{LS}(f)\right| \quad \text{and} \quad t^{rh}_{pSL}(f) = \frac{\left|\left(A^T_{1A}\right)_{rh}(f)\right|}{\left|\left(A^T_{1A}\right)_{ref}(f)\right|}\left|t^{ref}_{SL}(f)\right| \tag{2}$$

The corresponding FTI_t can thus be expressed as:

$$FTI\_t_{LS}(f) = \frac{\left|\left(A^T_{1B}\right)_{rh}(f)\right|}{\left|\left(A^T_{1B}\right)_{ref}(f)\right|} \text{ and } FTI\_t_{SL}(f) = \frac{\left|\left(A^T_{1A}\right)_{rh}(f)\right|}{\left|\left(A^T_{1A}\right)_{ref}(f)\right|} \tag{3}$$

2.2 The samples

The samples are silicon disks with a [100] crystallographic orientation. Silicon allows being machined controlled roughness and being treated so that its surface is hydrophobic. Before the experiment, the samples were subjected to a hydrophobic surface treatment : a liquid coating solution including octadecyltrichlorosilane (OTS). They have a diameter of 100 mm and a thickness of 10 mm. The thickness is sufficient to allow the different interface echoes to be separated. The excitation signals applied were impulses, in order to obtain the shortest possible echo durations, thereby avoiding the problem of overlapping echoes.

The simulated roughness of the "rough" samples must be as close as possible to the real case, that is, to the roughness resulting from mechanical machining. Nevertheless, to apprehend the complex phenomena involved into the gas pocket – ultrasound interaction and in order to establish a modelling, it is necessary to control the ratio ultrasound wavelength by gas pocket size and to fix a straightforward geometry. The roughness is thus simulated by means of cylindrical holes distributed over a hexagonal grid. The engraving is achieved using a RIE (Reactive Ion Etching) lithographic process with masks. Fourteen samples were produced, of which just one was kept smooth, and was used as the reference sample. When the samples were immersed in water, the cylindrical holes thus remained filled with gas (mainly air, together with a small quantity of water vapour) and the interface thus has a composite character.

Two criteria led to the selection of the depth of the cylindrical holes, and of the roughness of the "rough" surfaces. The hole depth must be greater than the protrusion depth of the liquid-gas interface curvature, to prevent this meniscus from touching the bottom of the hole. In addition, in order for the sample to be representative of the roughness resulting from mechanical machining, the hole depth must not be too large, and remain of the same order of magnitude as its diameter. For all of the samples, the chosen hole depth was 30 μm, and several diameters were investigated.

2.3 The parameters

2.3.1Parameters governing the roughness

The parameters characterising the controlled roughness of the "rough" surface of the samples are: the diameter d = 2r of the cylindrical holes, and the per unit area fraction of the cylindrical holes, ϕ_t . Although for a given sample, all the cylindrical holes have the same diameter, three different diameters were used: approximately 10, 20 and 30 µm. They were selected in order to respect two criteria: the first corresponds to the limits of the cylindrical hole engraving process, i.e. to a lower diameter limit of 10 µm. A smaller size of the holes would have to be more representative of typical machined surface roughness but below this value the circularity of the holes cannot be achieved by the machines used for the optical lithography and RIE engraving processes with thick samples. The second criterion is given by the 30 µm upper limit of the hole diameter, which corresponds to the maximum diameter (including a safety margin) able to guarantee the stability of the gas pockets when the surface is hydrophobic, with respect to the hydrostatic pressure imposed by the experimental conditions.

The fraction of cylindrical holes per unit area ϕ_t gives the ratio between the area of the disks representing the cylindrical hole apertures, and the total apparent area of the sample. The complement with respect to 1 of ϕ_t is noted τ. τ thus corresponds to the ratio between the area between the holes, and the area of the whole sample surface. When the sample is immersed in water, ϕ_t corresponds to the liquid-gas area fraction of the interface, i.e. $\phi_g = 1 - \tau$, of the composite interface, and τ corresponds to the actual solid-liquid interface area fraction. For example, for the surface of the reference sample, which has no holes, $\phi_g = 0$ and $\tau = 1$. The range of the parameters e, e' and r (Fig. 2) allows the factor τ to be varied between 0.5 % and 0.9 % (0.5; 0.7; 0.8; 0.9). This choice covers a useful range of values around 0.7 %. The latter value was identified[5] as the boundary between two regimes of ultrasound transmission.

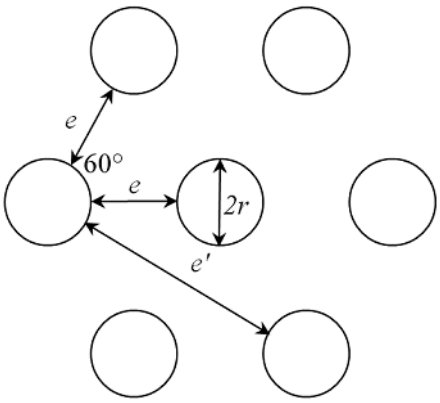

Figure 2. Description of the grid parameters of the holes

2.3.2 The parameter related to ultrasound: frequency

The transmission coefficient of the samples' composite interfaces are studied at two frequencies $f = \omega/(2\pi)$, one and five Megaherthz, each corresponding to the central frequency of two different pairs of transducers. The aim is to assess the frequency influence in a representative range of ultrasonic techniques used in sodium fast reactor. These frequencies are greater than the resonant frequencies of the gas pockets computed with expression (21) (see in a further section).. In order to limit the number of measurements, not all of the samples are tested with each of the transducers pairs. The transducer pair with a central frequency of 5 MHz is used with all of the samples, whereas the pair centered at 1 MHz is used only with the samples having cylindrical holes with a diameter of 30 μm.

2.4 Description of the experimental setup

The transducers and the selected sample are immersed in a tank filled with water at room temperature (around 20°C). They are positioned and aligned with respect to each other by means of two independent mechanical systems with several degrees of freedom. The first system allows the mutual position and orientation of the two transducers to be adjusted, and the second allows the perpendicularity of the sample surfaces (i.e. normal incidence) to be adjusted with respect to the ultrasonic beam. The transducers are not focused. The generated ultrasound signals are pulses. The pulse generation and acquisition system allows one or the other transducers to be used, indifferently, as the transmitter or the receiver. As shown in Fig. 3, the pulses to be transmitted by a transducer or recorded with the oscilloscope are controlled by two pulse generator/receivers, each being connected to a transducer on one side and to the oscilloscope on the other. The pulses transmitted through the sample can be sent and received in both directions. The experimental setup comprizes two separate signal generation and acquisition systems, in order to study the effect of the direction of ultrasound propagation with respect to the "rough" face of the samples, without changing the experimental setup.

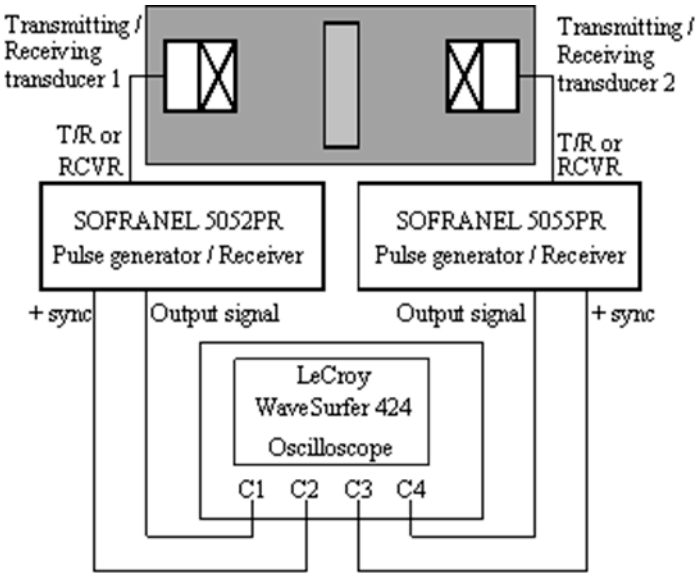

Figure 3. Drawing of the ultrasound signal generation and transmission system.

The distance between the transducers and the closest surface of the sample is adjusted to be at the limit of the near field for the 5 MHz frequency. For the 1 MHz pair of transducers, the signals are recorded in the far field at a distance of 72 mm from the sample, since the length of the near field is too short to be used with this experimental setup.

3. Model

In the case of the transmission of ultrasonic waves at normal incidence to the interface between two media, when an incident beam propagating in the first medium reaches the interface, part of this beam is reflected and the other part is transmitted into the second medium. In the ideal situation of a plane wave at normal incidence with respect to a smooth and flat interface, the pressure and velocity continuity equations at the interface allow the transmission coefficients of pressure tp and velocity tv (with tp = 1 + rp et tv = 1 + rv) to be determined as a function of the acoustic impedances Z of the two media (both of which are considered here to be elastic and isotropic):

$$t_p = \frac{2Z_2}{Z_1 + Z_2} = \frac{Z_2}{Z_1} t_v \tag{4}$$

where subscript 1 refers to medium 1 in which the incident and reflected waves propagate, and subscript 2 refers to medium 2, in which the transmitted wave propagates. Z is given by $Z = \rho c$ with ρ and c respectively the density and sound velocity of the medium. It is well known that at a solid-air or a liquid-air interface the velocity reflection coefficient is nearly equal to 1 (or -1 for the pressure reflection coefficient), and the wave is almost totally reflected at the interface.

From the acoustic point of view, a composite interface represents an intermediate case between a purely solid-liquid interface and that of a film of gas separating the solid from the liquid. However, as a result of the presence of roughness and a dispersed gaseous phase, the interaction between the ultrasonic wave and the interface becomes more complex, and the transmission coefficient can no longer be computed using expression (4). The gas pockets distributed in-between the purely solid-liquid contacts lead to scattering of the incident wave. As a result, the transmitted and reflected acoustic fields are the result of interactions between the wave and these scatterers. The nature of these interactions is governed by the ratio between the ultrasonic wavelength and the size of the scatterers, or in all likelihood by the resonant frequency of the scatterers in the case of gas pockets in contact with water.

The proposed interface stiffness model consists in the use of independent stiffnesses corresponding to the respective area fractions of the gas and the solid, and then applying an acoustic pressure amplitude which acts on each fraction. The stiffness of the gas area fraction is calculated from the “dynamic stiffness” of the gas pocket, which takes into account not only the static stiffness of the latter, but also an “inertial” component involving the acoustic excitation frequency and a radiative mass.

3.1 Behaviour of the gas pocket

In this section, we define the "dynamic stiffness" of the gas pocket, as a function of its geometry and the initial wetting conditions. Leighton[19] analysed the oscillatory dynamics of a gas pocket by comparing them with those of an ideal classical undamped mass-spring system. The ideal mass-spring oscillator differs from the real one, both in terms of stiffness and inertia. Actually, the stiffness is independent of the displacement when it occurs with very small amplitudes. In the ideal model the inertia is only related to the mass. However, in the real mass-spring oscillator, the acceleration of the mass also induces an acceleration of the spring. In addition, in order for the mass to be displaced, and for kinetic energy to be transferred to the

mass and the spring, kinetic energy needs to be applied to the volume of gas surrounding the system during its displacement. The inertial contribution of the surrounding fluid is defined in terms of the so-called radiative mass mr.

These differences with respect to an ideal mass-spring oscillator are amplified by the gas pocket. Indeed, we first demonstrate that the stiffness of the gas pocket depends on the displacement of its meniscus. In addition, for the real mass-spring oscillator, the radiative mass is generally negligible when compared with the inertia of the mass. On the other hand, for the gas inside a cavity within a liquid, the inertia associated with the acceleration of the liquid is much larger than that associated with the gas. As a consequence, the mass of the gas in the pocket will be considered to be negligible when compared to that of the radiative mass.

3.1.1 Geometry of the gas pocket

In order to simplify the theoretical problem, as well as the production of samples, the geometry of the studied gas pocket is approximated by a cylinder. Fig. 4 shows such a gas pocket, closed by a convex (as seen from the gas) liquid-gas interface, which will be referred to as a meniscus. This flexible interface is anchored to the edges of the cylindrical cavity and can change its curvature, since the equilibrium contact angle, noted θ, can vary between the maximum advancing θ_A and the minimum receding θ_R contact angles, which depend on the local surface roughness. A 90° corner represents a particular type of local roughness, which allows the transition from θ_R with respect to the horizontal surface, to θ_A with respect to the vertical surface, when the gas pocket volume decreases, as shown in Fig. 4.

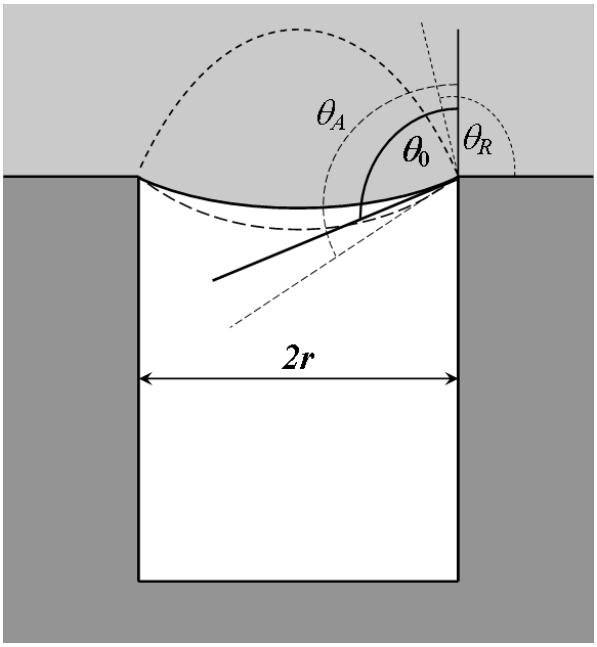

Figure 4. Initial state: the meniscus is anchored on the edges of the cavity and makes an angle θ_0 with its walls

3.1.2 Description of the gas pocket: pressure and curvature of the meniscus

The gas inside the pocket is assumed to behave polytropically[19]. By considering that, initially, and at equilibrium, the partial pressure p_G of the gas in the pocket is equal to the atmospheric pressure p_{atm}, for any motion of the meniscus we can write:

$$p_G V^{\kappa} = p_{atm} V_0^{\kappa} \text{ et } V = V_c + u_{LC} S_c + V_{cal}(\theta) \quad (5)$$

where V is the volume of the gas pocket, κ is the polytropic exponent, and the index 0 is used to indicate initial conditions. V_c is the volume of the cavity, such that: $V_c = S_c.h$ with h the cavity depth. S_c is the area of the cavity section. $S_c = \pi r^2$, where r is the radius of the cylinder. u_{LC} represents the displacement of the contact line inside the cavity. u_{LC} is nil when the meniscus lies at the edges of the cavity, and is negative when the meniscus is located between the edges and the bottom of the cavity. $V_{cal}(\theta)$ is the "algebraic" volume of the cap formed by the meniscus, and can be written as:

$$V_{cal}(\theta) = \frac{1}{3}\pi r^3 \frac{(2+\sin\theta)\cos\theta}{(1+\sin\theta)^2} \quad (6)$$

V_0 can then be written as: $V_0 = V(\theta = \theta_0, u_{LC} = 0)$. The displacement of the meniscus averaged over Sc is noted u_{GP} , and is defined by:

$$u_{PG}(\theta, u_{LC}) = u_{LC} + V_{cal}(\theta)/S_c \quad (7)$$

In the initial state $\theta_0 \leq \theta_A$, and when subjected to hydrostatic pressure with a liquid height h_L above the gas pocket, the equilibrium of the meniscus is given by the expression:

$$\cos\theta_0 = -\rho g h_L r / 2\gamma_{LV} \quad (8)$$

where ρ_L is the density of the liquid, g is the gravitational acceleration, and γ_{LV} is the surface tension of the liquid. The latter produces overpressure inside the pockets. Neglecting the vapour pressure of the liquid in the gas pocket, Laplace's law allows the equilibrium conditions of the meniscus to be written as:

$$p_G = p_A + p_{atm} + \rho_L g h_L + \gamma_{LV} C \quad (9)$$

where p_A is the fluctuating part of the liquid pressure near the meniscus. In the rest of the paper this pressure corresponds to the acoustic pressure of the ultrasonic wave generated by the transducer and C the curvature of the meniscus given by:

$$C = 2\cos\theta / r \quad (10)$$

By using expressions (5), (9) and (10), it can be shown that:

$$p_{atm}\left(\left(\frac{V_0}{V(\theta)}\right)^{\kappa}-1\right)=p_A+\rho g h_L+\frac{2\gamma_{LV}\cos\theta}{r} \tag{11}$$

3.1.3 Definition of the static stiffness per unit area K_{GPs} of the gas pocket

Unlike the method used by Leighton[27], the static stiffness per unit area K_{GPs} (G stands for Gas, P for pocket and s for static) is determined by using the Laplace pressure contribution, and taking the curvature of the meniscus into account, in addition to the resistance to compression and traction contributed by the gas in the pocket.

If the gas pocket is considered to be a spring with a stiffness per unit area K_{GPs} , then it will respond to a small displacement du_{GP} of the meniscus by exerting a pressure $-K_{GPs}\, du_{GP}$. If dp represents a small variation in the pressure with which the liquid pushes on the meniscus, such that $dp > 0$ for overpressure and $dp < 0$ for depression, then K_{GPs} can be written as:

$$K_{GPs}=-\frac{dp}{du_{GP}}. \tag{12}$$

When at rest, if the meniscus is anchored to the edges of the cylindrical cavity and adopts an equilibrium angle θ, expression (12) can be rewritten as:

$$K_{GPs}=-\left(\frac{dp_A}{d\theta}\right)_{\theta_0}\left(\frac{dV(\theta)}{d\theta}\right)_{\theta_0}^{-1}\left(\frac{dV}{du_{GP}}\right)_0 \tag{13}$$

If we consider the case in which the meniscus is anchored to the edges of the cavity, such that $u_{LC} = 0$, from expressions (5) and (7) it follows that:

$$\left(\frac{dV}{du_{GP}}\right)_0 = S_c \tag{14}$$

from (11):

$$\left(\frac{dp_A}{d\theta}\right)_{\theta_0} = -\frac{\kappa p_{atm}}{V_0}\left(\frac{dV}{d\theta}\right)_{\theta_0} + \frac{2\gamma_{LV}\sin\theta_0}{r} \tag{15}$$

and from (5) and (6):

$$\left(\frac{dV}{d\theta}\right)^{-1}_{\theta_0} = -\frac{(\sin\theta_0 + 1)^2}{\pi r^3} \tag{16}$$

Thus, for the case in question of a gas pocket in a cylindrical cavity, expression (13) lead to:

$$K_{GPs} = S_c\left[\frac{\kappa p_{atm}}{V_0} + \frac{(\sin\theta_0 + 1)^2}{\pi r^3}\frac{2\gamma_{LV}\sin\theta_0}{r}\right] \tag{17}$$

3.1.4 Definition of the radiative mass of the gas pocket

The meniscus of a gas pocket inside a cylindrical hole can, to a certain extent, be described as a baffled flat-top piston. It is indeed assumed that the liquid driven by the displacement of the meniscus during the transit of an acoustic wave has an effective mass very close to that which would be driven by a baffled flat-top piston. This supposes the displacement of the contact line to be negligible. It must also be assumed that the curvature of the meniscus, throughout the acoustic excitation, remains very small. Pierce[28] gives an expression for the radiative mass m_r of a baffled piston, for ka << 1, where k is the wave number of the acoustic wave and a is the radius of the piston, which here corresponds to the parameter r:

$$m_r = 8\rho_L r^3/3 \tag{18}$$

ka ≈ 0.06 for the least objectionable experimental case (r = 15 µm and f = 1 MHz) and ka ≈ 0.32 for the most objectionable experimental case (r = 15 µm and f = 5 MHz).

The radiative mass per unit area M_r is obtained by dividing the radiative mass m_r by the area S_c:

$$M_r = 8\rho_L r / 3\pi \tag{19}$$

3.1.5Definition of the "dynamic stiffness" of the gas pocket

If the gas pocket is considered to be an undamped oscillator with a stiffnes per unit area K_{GPs} and mass per unit area M_r, the equation governing the displacement of the meniscus is given by:

$$M_r \ddot{u}_{GP}(t) + K_{GPs} u_{GP}(t) = -p_A(t) \tag{20}$$

This is a conservative behaviour in which viscous friction losses are neglected. The natural angular frequency of the gas pocket ω_{GP} can then be expressed by:

$$\omega_{GP} = \sqrt{\frac{K_{GPs}}{M_r}} \tag{21}$$

If p_A is a harmonic function, complex notation can be used to express equation (20) as:

$$M_r \ddot{y} + K_{GPs} y = -P_A e^{i\omega t} \tag{22}$$

where y is the complex equivalent of u_{PG}. The solution to $y = Ye^{i\omega t}$, where ω is the excitation angular frequency (of the ultrasound), leads to:

$$\left(M_r \omega^2 - K_{GPs}\right) Y = P_A \tag{23}$$

Here, $K_{GPs} - M_r\omega^2$ represents the "dynamic stiffness" per unit area of the gas pocket. This “dynamic stiffness” takes the static stiffness of the gas pocket, as well as an “inertial resistance” into account, the latter being related to the acoustic excitation frequency and the radiative mass.

The displacement u_{GP} can thus be expressed as:

$$u_{GP} = \frac{p_A}{\left|M_r\omega^2 - K_{GPs}\right|} \quad . \qquad (24)$$

3.2 Use of a mass-spring model to represent an imperfect interface

The quasi-static mass-spring model, used to describe ultrasound transmission at an imperfect interface, is based on the description given by Baik and Thompson[10] (Fig. 5.a). By assuming the scatterers on such an imperfect interface, as well as the spaces in-between the scatterers, to be small in comparison with the wavelength, the transmission and reflection of ultrasound at the interface can be predicted by describing the latter as the combination of a spring of stiffness per unit area K, and a distributed mass per unit area M.

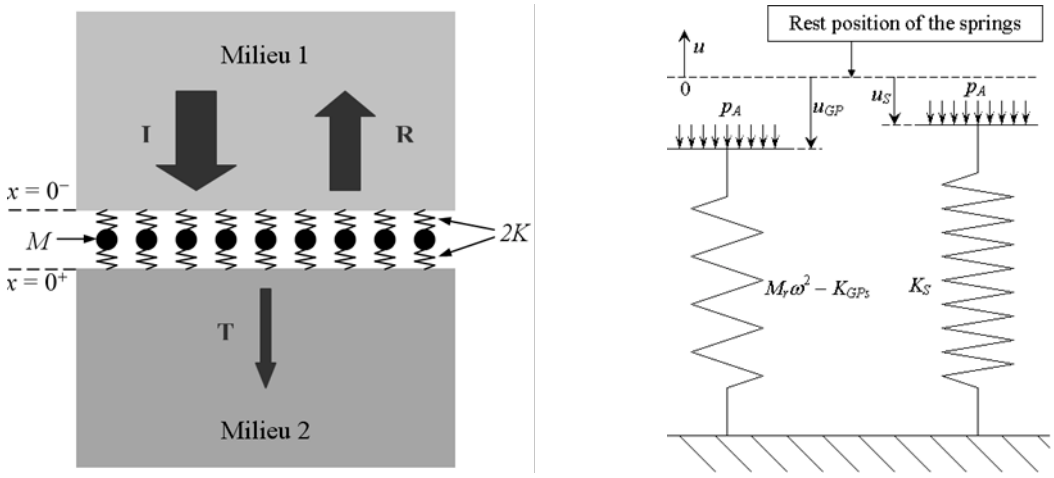

Figure 5 – (a) Mass-spring model of the imperfect interface separating medium 1 from medium 2, incident, transmitted, and reflected waves: I, T and R; (b) conceptual system of the effective spring equivalent to two independent springs: that of the gas area fraction (left) and solid area fraction (right).

With the area fraction of the solid-liquid interface given by τ, and the respective densities of the solid and the gas given by ρ_S and ρ_G, the density ρ_I of a composite interfacial layer can be expressed as:

$$\rho_I = \tau\rho_S + (1 - \tau)\rho_G \quad (25)$$

If h is the height of the interface, M is given by [10] :

$$M = \int_0^h (\rho_I - \rho_S)dx = h(\tau - 1)(\rho_S - \rho_G) \quad . \quad (26)$$

In the proposed model, illustrated in Fig. 5.b, the interfacial stiffness corresponds to that of an effective spring equivalent to two springs: that corresponding to the solid area fraction, and that corresponding to the gas area fraction. The stiffness of the latter is calculated on the basis of the "dynamic stiffness" of the gas pocket.

The sign convention for displacements has arbitrarily been chosen according to the convention shown in Fig. 5.b. Thus, as shown in the drawing of Fig. 5.b, the pressure p_A is positive and the displacements u_{GP} and u_S are negative. When an acoustic pressure is applied, and is represented by a static constraint, the displacement of the interface u_I can be considered to be a variation in thickness of the composite interfacial layer, i.e.:

$$u_I = \phi_S u_S + \phi_G u_{GP} \quad (27)$$

where u_{GP} is the displacement of the meniscus of each gas pocket given by (24), u_S is the displacement, more precisely the variation in thickness of the solid fraction contained in the interfacial layer, such that it can be expressed as:

$$u_S = -\frac{p_A}{K_S} \quad (28)$$

Since silicon is a cubic crystal with elastic constants such as $C_{11} = C_{22} = C_{33}$ and since the longitudinal sound wave propagation direction is parallel to one of the crystal symmetrical axis, K_S can be calculated by the relationship:

$$K_S = \frac{C_{11}}{h} \quad . \qquad (29)$$

The displacement u_I can be written as the sum of the displacement u_S, which would have existed if the interface been "perfect", i.e. completely solid – liquid (no hole and gas pocket), plus the extra displacement Δu due to local deformation of the composite interface (solid layer with a distribution of holes in which the solid is replaced by a gas). The extra displacement Δu can therefore be expressed as:

$$\Delta u = u_I - u_S \qquad (30)$$

Making use of (24) and (28), the expression (30) becomes:

$$\Delta u = p_A (1-\tau)\left(\frac{1}{K_{GPs}} + \frac{1}{M_r \omega^2 - K_{GPs}}\right) \qquad (31)$$

Where K_{PGs} is given by expression (17) and M_r by expression (19).

The effective stiffness of the spring K is positive, and equal to $p_A/\Delta u$ when p_A and Δu are of the same sign, i.e. when $\omega > \omega_{GP}$, and is equal to $-p_A/\Delta u$ when p_A and Δu are of the opposite sign, i.e. when $\omega < \omega_{GP}$. K is thus given by[10] :

$$K = \left|\frac{p_A}{\Delta u}\right| = \left|\frac{1}{\tau - 1}\frac{K_S\left(M_r\omega^2 - K_{GPs}\right)}{K_S + \left(M_r\omega^2 - K_{GPs}\right)}\right| \qquad (32)$$

Equations (26) and (32) are used to compute the coefficient of transmission tp of the ultrasonic wave through the composite interface by using the Baik and Thompson expression[10]:

$$t_p = \frac{2Z_2\left(1+\frac{M\omega^2}{4K}\right)}{(Z_1+Z_2)\left(1-\frac{M\omega^2}{4K}\right)+i\omega\left(\frac{Z_1Z_2}{K}+M\right)}. \quad (33)$$

4. Results and discussion

In order to reduce the electronic noise, the recorded signal is taken as the average of 1024 raw signals. Each echo is temporally isolated, and then Fourier transformed. Using Eq. (3), FTI_t_{SL} and FTI_t_{LS} are computed for each sample. Taking the values of FTI_t for the central frequencies of the 1 MHz and 5 MHz transducers, the corresponding FTI_$t_{SL}(\tau)$ curves are plotted in Fig. 6, for the three values of cylindrical hole diameter (only 30 µm at 1 MHz). The corresponding FTI_$t_{SL}(\tau)$ curves are not shown because the results obtained in the solid-to-liquid direction are almost identical to those obtained in the liquid-to-solid direction. This indicates that the transmission coefficient of the composite interface is the same for both directions of wave propagation.

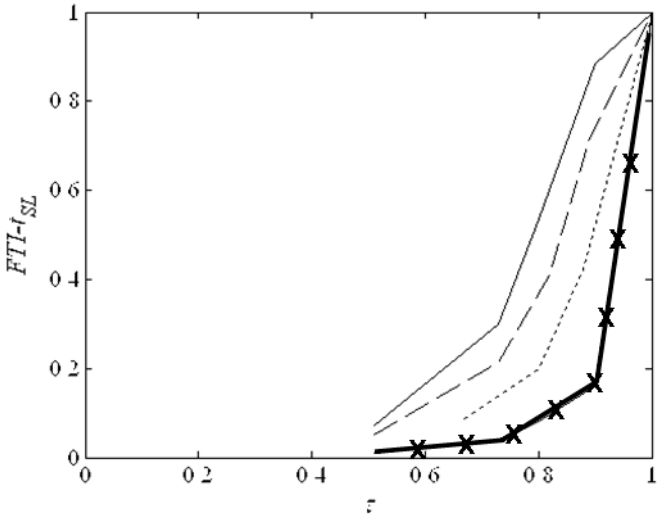

Figure 6. FTI_t as a function of τ in the solid-to-liquid direction.

thin black: f = 5 MHz; thick black with x ticks : f = 1 MHz ;

continuous line: d = 30 µm; dashed line: d = 20 µm; dotted line: d = 10 µm. and d =30 µm.

As observed in the previous study[7], FTI_t increases with τ. In addition, this work shows that, for the same value of gas area fraction, FTI_t increases with the frequency, and with the diameter of the cylindrical holes. In other words, it increases with the parameter d/λ. This tendency could be explained by the fact that when d/λ increases, the excitation moves away from the resonance frequency of the gas pockets.

The theoretical $FTI\_t_{SL}(\tau)$ curves calculated with our model are presented in Fig. 7 using input data listed in Table 1. They are plotted using Eq. (1) in which Eqs (4) and (33) have been implemented respectively for the reference sample and for the "rough" hydrophobic sample replacing subscripts "1" and "2" respectively by "S" and "L".

Elastic constant of the solid (silicon at 20°C and p_{atm})	C_{11}	165.6 GPa
Velocity of sound waves in the gas (air at 20°C and p_{atm})	c_G	344 m/s
Velocity of sound waves in the liquid (water at 20°C and p_{atm})	c_L	1480 m/s [29]
Velocity of longitudinal sound waves in the solid (silicium at 20°C and p_{atm})	c_S	8430 m/s [30]
Gravitational acceleration	G	9.81 m/s2
Cavity (or hole) depth	H	30 µm
Liquid height above the gas pocket	h_L	100 mm
Atmospheric pressure	p_{atm}	101350 Pa
Cylindrical cavity (or hole) radius	R	5, 10 and 15 µm
Surface tension of the liquid (water at 20°C and p_{atm})	γ_{LV}	0.07 J/m2
gas (air at 20°C and p_{atm}) polytropic exponent	κ	1
density of the gas (air at 20°C and p_{atm})	ρ_G	1.204 kg/m3
density of the liquid (water at 20°C and p_{atm})	ρ_L	1000 kg/m3
density of the liquid (silicon at 20°C and p_{atm})	ρ_S	2329 kg/m3
Equilibrium contact angle of the meniscus in the initial state (plane meniscus at equilibrium)	$\theta 0$	90°

Table 1. Input data for the model.

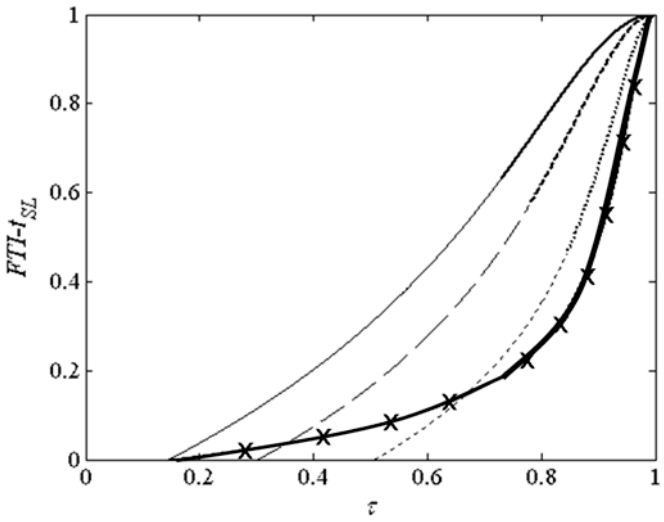

Figure 7. Curves for FTI_t_{SL} as a function of τ at 1 MHz (black line) and 5 MHz (black line with x ticks) red line) obtained from our model. Continuous line: d = 30 µm; dashed line: d = 20 µm; dotted line: d = 10 µm

In the region corresponding to the bold lines, resonance effects are weak, whereas in the region in which fine lines are used, the errors resulting from the mass-spring model may be significant[7].

Figs. 6 and 7 shows that there is a good agreement between the model and the experiment. The drop in transmission associated with an increase in gas area fraction is rather close to that observed experimentally. In addition, the predicted trend for variations in transmission as a function of the ultrasound wave frequency and the diameter of the gas pockets is in good agreement with the experimental results. However, this model slightly overestimates the ultrasound transmission. One possibility for improving the model would be to include the effect of viscous dissipation in the form of a damping in the mass-spring models, as well as the acoustic scattering due to the diffraction of ultrasonic waves on the edges of the holes.

This modelling approach corresponds to a controlled roughness and should be developped in further works to get closer to the real roughness. It would be possible to obtain a 3D description of a surface to have a complete roughness mapping. This 3D description should be completed by a modelling approach to obtain for example an equivalent τ parameter as several parameters should be taken into account (depth but also slopes). Nevertheless the figure 7 gives yet useful information for industrial use. Using liquid sodium parameters and with an estimation of τ parameter it would be possible to estimate the efficiency of the transducer in real configurations (transducers immersed in liquid sodium).

5. Summary

The aim of the work presented in this paper is to study the ability of ultrasound waves to go through a composite interface. An experimental study has been undertaken using water as the liquid and hydrophobic oxidized silicon for the solid surfaces on which a distribution of small calibrated holes have been grooved, which remain filled with gas when the surface is in contact with water.

The experimental work is complemented by a theoretical approach intended to be predictive. In this model, the interface has been considered to be a partial contact interface between the liquid and the solid. Hence a distributed mass and spring model has been used to determine the transmission coefficient of such an interface. In order to determine the stiffness of the distributed equivalent spring of the entire interface, the behaviour of a gas pocket under the influence of ultrasound has been predefined.

The experimental and predicted results have been found in semi-quantitative agreement. Experimental and calculated drop of the ultrasound transmission associated with an increase in gas area fraction are rather close to each other. In addition, the trend for variations in transmission as a function of frequency and the diameter of the gas pockets are similar. The overestimation of the ultrasound transmission by the model could be corrected by taking into account viscous dissipation and scattering effects at the edges of the cavities.

It has been showed that, in addition to the gas area fraction, the size of the diffusers that are gas pockets and the ultrasonic frequency excitation have a significant influence on the transmission coefficient at the interface. Therefore, this simulated study brings new elements of understanding about the transmission drop at the interface between an ultrasonic transducer and the liquid sodium.

Aknowledgments

The authors express their gratitude to Jean Luc BERTON who contributed to the modelling approach by his advices and by sharing his great experience in the use of ultrasound in liquid sodium.

References

[1] P. Martin, P. Anzieu , J. Rouault, et al., Nucl. Eng. Tech., **39**, 237 (2007)

[2] F. Baqué, G. Rodriguez, N. Jardin N., J.M. Carpreau, J.M. Augem, J. Sibilo, 1st Int. Conf. ANIMMA, Marseille (2009)

[3] G. Gobillot, F. Baqué, C. Lhuillier, P.H. Brau, M.A. Ploix, J.M. Augem, J.Fr. Saillant, 1st Int. Conf. ANIMMA, Marseille (2009)

[4] K. Paumel, O. Descombin, J. Moysan, G. Corneloup, J.-M. Augem, 1st Int. Conf. ANIMMA, Marseille (2009)

[5] K. Paumel, J. Moysan, M.Autric, C. Gueudré, G. Corneloup, F. Baqué, Nucl. Eng. Des., **239**, 2272 (2009)

[6] D. Chatain, C. Lesueur, J.P. Baland, Langmuir, **22**, 4230 (2006)

[7] C. Lesueur, J. Moysan, G. Corneloup, F. Baqué, NDT&E Int., **41**, 155 (2008)

[8] K. Kendall, D. Tabor, Proc. Roy. Soc. London, **323**, 321 (1971)

[9] H.G. Tattersall, J. Appl. Phys., D6, 819 (1973)

[10] J.-M. Baik, R.B. Thompson, , J Nondestr Eval, **4**, 177 (1984)

[11] A. Baltazar, S.I. Rokhlin, C. Pecorari, J. Mech. Phys. Solids, **50**, 1397 (2002)

[12] F.J. Margetan, R.B. Thompson, J.H. Rose, T.A. Gray, J. Nondestruct. Eval. **11**, 109 (1992)

[13] N. F. Haines, CEGB Berkeley Nuclear Laboratories, Report RD/B/N4744 (1980)

[14] B.W. Drinkwater, R.S. Dwyer Joyce, P. Cawley, Proc R Soc Lond Ser A: Math Phys Eng Sci; **452,1955**, 2613 (1996)

[15] R.S. Dwyer-Joyce, B.W. Drinkwater, A.M. Quinn, J. Tribol., **123**, 9 (2001)

[16] A.M. Quinn, B.W. Drinkwater, R.S. Dwyer-Joyce, Ultrasonics, **39**, 495 (2002)

[17] R. Thomas, B.W. Drinkwater, D. Liaptsis, J. Acoust. Soc. Am., **117**, 2 (2005)

[18] A.I. Lavrentyev, A. Baltazar, S.I. Rokhlin, Rev. Prog. Quant. Nondestr. Eval., **17**, 1379 (1998)

[19] C.J. Brotherhood, B.W. Drinkwater, S. Dixon, Ultrasonics, **41**, 521 (2003)

[20] Y.C. Angel, J.D. Achenbach, J Appl Mech, **52**, 33 (1985).

[21] R.S. Dwyer-Joyce, T. Reddyhoff, B.W. Drinkwater, Tribol. Trans., **47**, 366 (2004)

[22] X. Guo, D. Zhang, J. Wu, J. Appl. Phys., **108**, 034902 (2010)

[23] J.Y. Kim, J.S. Lee, J. Appl. Phys., **101**, 043501 (2007)

[24] P. Attard, S. J. Miklavcic, Langmuir, **17**, 8217 (2001)

[25] E. Charlaix, H. Gayvallet, Jour. de Phys. II, **2,** 2025 (1992)

[26] Z. Guo, A. G. Jones,H. Hao, B. Patel, N. Li, J. Appl. Phys., **101**, 043501 (2007)

[27] T.G. Leighton, P.R. White, M.A. Marsden, Acta Acustica, **3-6,** 517 (1995)

[28] A.D. Pierce, Acoustical Society of America (1991)

[29] V.A. Del Grosso, C.W. Mader, J. Acoust. Soc. Am., **52,** 1442 (1972)

[30] S.D. Lambade, G.G. Sahasrabudhe, S. Rajagopalan, Phys. Rev. B, **51** (1995).